Structural Engineering and Mechanics, *Vol. 57, No. 5 (2016) 785-808*
DOI: http://dx.doi.org/10.12989/sem.2016.57.5.785

Experimental study on innovative tubular web RBS connections in steel MRFs with typical shallow beams

Aboozar Saleh[a], Seyed M. Zahrai[*] and Seyed R. Mirghaderi[b]

School of Civil Engineering, the University of Tehran, Iran

(Received July 20, 2015, Revised November 9, 2015, Accepted December 10, 2015)

Abstract. An innovative Reduced Beam Section (RBS) connection, called Tubular Web RBS connection (TW-RBS), has been recently introduced and its performance has been numerically investigated in some earlier studies. The TW-RBS connection is a kind of accordion-web RBS connection in which part of the flat web of the beam is replaced by a steel tube at the expected region of the plastic hinge. This paper presents experimental results of three TW-RBS connections under cyclic loading. Obtained results indicated that TW-RBS reduces contribution of the beam web to the whole moment strength and creates a ductile fuse far from components of the beam-to-column connection. Besides, TW-RBS connection can increase story drift capacity up to 9% in the case of shallow beams which is much more than those stipulated by the current seismic codes. Based on the experimental results, the tubular web in the plastic hinge region improves lateral-torsional buckling stability of the beam such that only local buckling of the beam flange at the center of the reduced section was observed during the tests. In order to achieve a better understanding, behavior of all TW-RBS specimens are also numerically investigated and compared with those of experimental results.

Keywords: cyclic testing; special moment frame; reduced beam section; tubular web RBS (TW-RBS); test specimens; shallow beams

1. Introduction

The unexpected local and brittle damages of beam-to-column connections of steel moment-resisting frames in the Northridge and Kobe earthquakes have resulted in significant concerns regarding reliability of the fully restrained beam-to-column connections. Extensive experimental campaigns have been carried out by various researchers as part of the SAC Steel Project. A brief review of these studies can be found in FEMA 350 (2000). The high stress concentration at the welded web and flanges and the vulnerability of the connection to the large ductility demand are considered as those two critical factors causing such failures (FEMA 350 2000). A common way to solve the problem is to reduce the ductility demand and alleviate strain concentration at the welded regions.

In order to address the abovementioned concerns, different techniques have been investigated

*Corresponding author, Professor, E-mail: mzahrai@ut.ac.ir
[a]Ph.D. Student, E-mail: aboozar.saleh@ut.ac.ir
[b]Assistant Professor, E-mail: rmirghaderi@ut.ac.ir

http://www.techno-press.org/?journal=sem&subpage=8 ISSN: 1225-4568 (Print), 1598-6217 (Online)

in earlier studies. Reduced Beam Section (RBS) moment connection is one of the most economical and practical prequalified connections among the post-Northridge ones. RBS connection was proposed by intentionally reducing the plastic flexural capacity of the beam section at a region away from the column face. In this way, formation of the plastic hinge would occur at a predetermined point selected by the designer (FEMA 350 2000).

This feature of the RBS can lead to significant reduction in the developed demands on the beam-column connection as well as its components such as panel zone, continuity plate, etc.

Cutting and drilling of the flanges are two common methods of reducing the plastic moment capacity of the beam. During 1996 to 1998, SAC committee (FEMA-355D 2000) showed that the radius cut RBS connection has better behavior compared to other shapes of flange cuts and also behavior of the connection depends on the beam depth. Various parameters of usual RBS connection have been studied by others. In a recent study, Han and Moon (2009) have suggested that in the case of deep beams (with span to depth ratios of less than 10) in which their flanges contribute less than 70% to the overall bending capacity, web bolting in the conventional RBS connection is not recommended. Pachoumis *et al*. (2010) studied cyclic behavior of RBS moment connections through experimental and numerical analyses. They showed that use of RBS connections in European sections requires some modifications on the RBS geometric parameters. Connection with web reduction is another type of reduced beam section connections. For example, behavior of RBS connections with web circular holes has been investigated by Yang and Yang (2009). Behavior of beams with perforated webs has been also studied by Tsavdaridis and D'Melloon (2012). They have focused on beams with elliptical web opening and concluded that such details can lead to satisfactory results both in terms of technical and constructional points of view.

Most conventional RBS connections and those with web reduction would reduce out-of-plane stiffness of the beam. In other words, beams with conventional RBS connections are vulnerable to lateral-torsional buckling. As reported by Naeim (2001), RBS connections usually experiences web local buckling first, followed by lateral-torsional buckling and finally flange local buckling. The problem of lateral stability becomes much more apparent in the case of deep beams which are common in tall buildings. The amplitude of the lateral-torsional buckling tends to be larger when the RBS is used for deep beams, giving rise to impose twisting on the columns. Naeim (2001) suggested that in these cases lateral bracing should be provided near the reduced section region. To resolve this problem Wilkinson *et al*. (2006) have evaluated a new detail by which the web height reduction near the connection of beam-to-column was achieved. The experimental results approved plastic rotation capacity of more than 5%. Ricels *et al*. (2003) have also presented ductile details for welded unreinforced moment connections. Morrison *et al*. (2015) experimentally studied an innovative technique for reduced flexural capacity. The technique involves strength reduction of specified regions of the beam flanges by exposing them to high temperatures followed by slow cooling. Analogous to the reduced beam section (RBS) connection, yielding and plastic hinge formation is promoted in the heat-treated beam section (HBS). HBS connection does not sacrifice elastic stiffness or buckling resistance as does the RBS. The results showed that HBS connection experienced story drifts as high as 6% without weld or near weld fracture.

Connection with accordion web is another kind of RBS detail in which the accordion web is made by replacing part of the flat web with a corrugated web at the selected location of the beam plastic hinge. The corrugated web has adequate shear strength while its provided moment strength and flexural stiffness are negligible due to the fact that in the longitudinal direction, stiffness of the corrugated web is small. As a result, in the case of beams with accordion webs, the whole flexural

capacity would be due to contribution of the flanges. Moreover, accordion webs have large out-of-plane stiffness and would not damage lateral-torsional stability of the beam. Mirghaderi *et al*. (2010) discussed and evaluated connections of corrugated web reduced cross section in shallow beams. Observed experimental results indicated that the proposed connection can tolerate story drifts of up to 8% without experiencing significant strength deterioration. In another experimental campaign, Saleh *et al*. (2016a, b) have studied tubular web RBS connection (TW-RBS) for deep beams. No lateral-torsional buckling or strength degradation was observed in the specimens with TW-RBS connections even during large story drift. In another study, they used two accordion cells (two steel tubes) in deep beams; in order to extend the plastic zone on the beam flange and increase related energy dissipation. Obtained results of two test specimens revealed that TW-RBS with two accordion cells increases story drift capacity up to 6% in the case of deep beams and reduce 10% of demands at the beam-to-column connection by increasing plastic hinge length on the beam flange. It should be pointed out that TW-RBS provides superior performance compared with AW-RBS connection in terms of low-cycle fatigue, by changing sharp corners of angles to arc shape of the tubular web in beam section.

In this study, hysteretic behaviors of three shallow beams with interior TW-RBS connections are experimentally and numerically investigated and the main results are presented in the subsequent sections.

2. Proposed connection: TW-RBS in shallow beam

The assembly and related configuration of the proposed connection are illustrated in Fig. 1. As shown in the figure, in a limited zone near the column face the flat web of the beam would be replaced by a steel tube. The beam is connected to the column face by Complete Joint Penetration (CJP) welds to develop a full capacity rigid connection. Based on the small stiffness along the longitudinal direction of the corrugated sheet, contribution of the beam web within the corrugated region is negligible in the overall flexural capacity of the beam. Therefore, the proposed connection is a kind of RBS connection and would be called Tubular-Web RBS connection (TW-RBS) hereafter.

The following are the main advantages of the TW-RBS connection:

- TW-RBS can reduce plastic strain demand near the CJP welds and effectively concentrate the plastic strains within the reduced region.
- The flexural strength capacity of the plastic hinge can easily be estimated in the reduced region based on the beam flanges, as contribution of the tubular web can be ignored.
- The most important feature of the tubular web is to improve the out-of-plane stiffness of the beam at the reduced region. Moreover, local buckling of the flange would be delayed due to presence of two restrained edges for the flange at the plastic hinge region.

3. Experimental study

In order to validate the analytical results, a set of quasi-static cyclic tests has been carried out to experimentally study behavior of the proposed TW-RBS moment connections in shallow beams. Also the results are compared to experimental results of AW-RBS (the proposed connection by Mirghaderi *et al*. 2010).

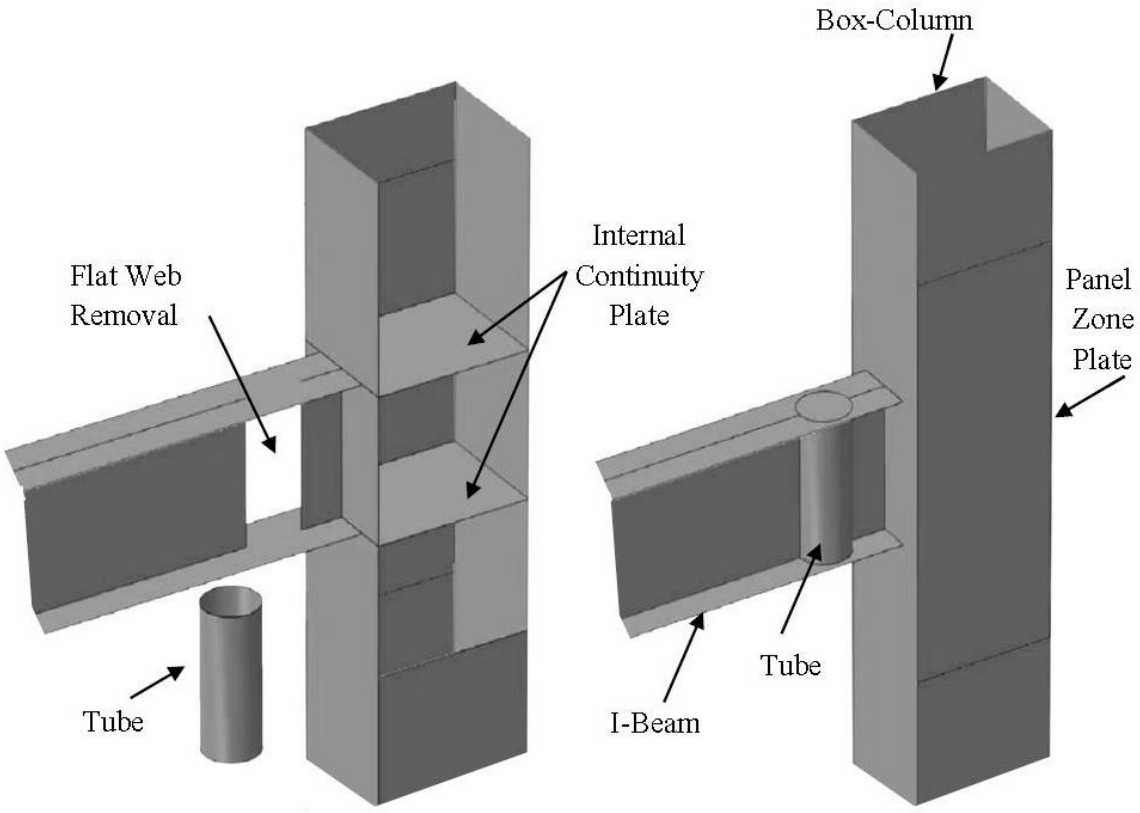

Fig. 1 Assembly and related configuration of the proposed connection

3.1 Test specimens

In this research, three 2/3 scale relatively identical specimens with TW-RBS connections were designed to be fabricated and tested. Similar to AW-RBS specimens (Mirghaderi *et al*. 2010), adopted specimens in this study are interior connection subassemblies with beams attached to the column opposite faces. In the subassemblies, half of the lower and upper columns were chosen as the vertical elements and half of the right and left beams were selected as the horizontal elements. All of the specimens were fabricated by a commercial fabricator.

The specimens consist of box-column (built-up 200×160×10) and IPE180 (Table 1) for beams. To construct TW-RBS connections, the beam webs were removed by a hand cutting torch and ground by a hand grinder. The tube used to replace the removed segment in test specimens has outside diameter of 76 mm and wall thickness of 3.3 mm in specimen 1 (SP1), outside diameter of 73 mm and wall thickness of 5.5 mm in specimens 2 and 3 (SP2 & SP3). Two types of steel tube were used in the specimens to explore the possible effects of the tube geometry at the cyclic behavior of the proposed connection. The geometrical dimensions are 2150 mm for the vertical members, acting as the columns, and 3290 mm (distance between the roller boundary conditions of the two beams) for the horizontal members which represent beam elements. The specimens are designed to satisfy the strong column-weak beam criterion to ensure a plastic mechanism in the

Table 1 Section properties for IPE180

Section	A_b ($m^2\times10^{-4}$)	d_b ($m\times10^{-2}$)	b_f ($m\times10^{-2}$)	t_f ($m\times10^{-2}$)	t_w ($m\times10^{-2}$)	Z_b ($m^3\times10^{-6}$)
IPE180	23.9	18	9.1	0.8	0.53	166

Cross-section Area: A_b Depth of beam: d_b
Width and Thickness of flange: b_f and t_f Thickness of web: t_w
Plastic modulus of unreduced section: Z_b

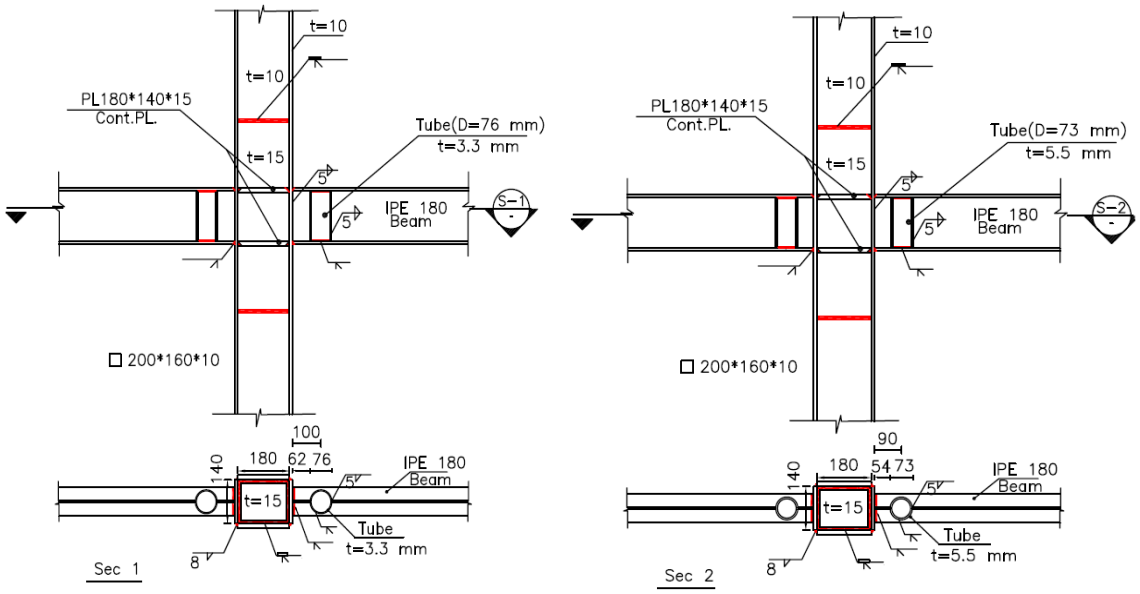

(a) SP1 (b) SP2 & SP3

Fig. 2 Test Specimens of TW-RBS connection and related details.

beam. Besides, all sections are selected to be seismically compact.

Except for the corrugated web, other details are similar to those previously used for the AW-RBS specimens by Mirghaderi *et al*. (2010). Again note that in the AW-RBS specimens, the corrugated web was two symmetric angles (2L50×50×4) while in the proposed TW-RBS, the corrugated web would be achieved through a tubular section. The TW-RBS connection details of all specimens prepared in a fabrication shop are illustrated in Fig. 2.

The beam flanges were connected to the column face by applying a prequalified CJP groove welding without backing bar with a root pass and a reinforcing fillet. CJP groove welds were applied between the continuity plates and the box-column while steel backing bars were left in place. Also CJP groove welds were used to connect the web tubes to the beam flanges. Other connections, such as beam web to the box-column, tubes to beam web, are made by fillet welding. The electrode E7018 with ultimate stress of 420 MPa is used for all welds. All groove welds were ultrasonically checked and all fillet welds were visually inspected by a licensed inspector. The beams, columns, continuity plates were all of A36 steel with nominal yield stress of 240 MPa. The mechanical properties of steel coupons, obtained from the specimens, are presented in Table 2, in accordance with ASTM A370 standard for tensile testing of steel.

Table 2 Mechanical properties of steel coupons

Test Specimen	Member	Coupon	Yield strength (MPa)	Tensile strength (MPa)	Elongation (%)
1	Beam	Flange	286	430	39
1	Beam	Web	312	438	39
1	Tube	-	369	395	32
2,3	Beam	Flange	325	489	26
2,3	Beam	Web	328	468	33
2,3	Tube	-	649	744	22
1,2,3	Box-Column	Web & Flange Plates	266	400	44
1,2,3	Box-Column	Panel zone & continuity plates	283	407	45.5

Table 3 Beam design control at the column face

Test Specimen	$Z_{TW\text{-}RBS}$ ($m^3\times10^{-6}$)	$M_{TW\text{-}RBS}$ (kN-m)	L ($m\times10^{-2}$)	e ($m\times10^{-2}$)	M_f (kN-m)	Z_bF_{ye} (kN-m)	α	$e+d_c/2$ ($m\times10^{-2}$)	$\sum M_{pb}$ (kN-m)	$\sum M_{pc}$ (kN-m)	$\sum M_{pc}/\sum M_{pb}$
1	127.21	50.38	144.5	10	53.87	59.76	0.901	20	114.7	205.44	1.79
2&3	131.44	52.05	145.5	9	55.27	59.76	0.925	19	117.7	205.44	1.75

Plastic section modulus of the TW-RBS: $Z_{TW-RWS} = Z_{flange} + (1 - \frac{2(\frac{t_c}{t_f})^2}{(\frac{D}{t_f})})Z_{web}^{flat}$

Thickness of pipe: t_c Diameter of pipe: D Thickness of flat web: t_f

Expected moment in plastic hinge location: $M_{TW-RBS} = 1.1R_yZ_{TW-RBS}\,\mathrm{F_y}$

Distance between the centerline of nearest pipe to column to middle span: L

Distance between the centerline of nearest pipe to column to the column face: e

Beam moment at the column face location: $M_f = M_{TW-RBS}\frac{(\mathrm{L+e})}{\mathrm{L}}$

Plastic modulus in unreduced beam and column sections: Z_b and Z_c

Moment ratio at the column face: $\alpha = \frac{M_f}{Z_bF_{ye}}$ Column depth: d_c

Beam moment in center of column: $\sum M_{pb} = M_f\frac{(L+e+d_c/2)}{(L+e)}$ Column plastic moment: $\sum M_{pc} = \sum Z_cF_{yc}$

3.2 Design procedure of the TW-RBS connection

Flexural design of the TW-RBS connection is presented in Table 3. The expected yield stress (F_{ye}) was calculated based on a nominal yield stress of 240 MPa and R_y of A36 steel hot-rolled structural shapes, which is 1.5 per AISC (2010). The ratio of maximum moment demand at the column face to the nominal plastic strength (α) has been obtained 0.901 for SP1 and 0.925 for SP2 and SP3. The recommended value for this parameter in design of common reduced beams is 0.9 (Engelhardt *et al*. 1998).

3.3 Test setup and instrumentation

The experimental procedure was carried out at the structural laboratory of the Building and Housing Research Center of Iran. An overall view of the test set-up and dimensions of the

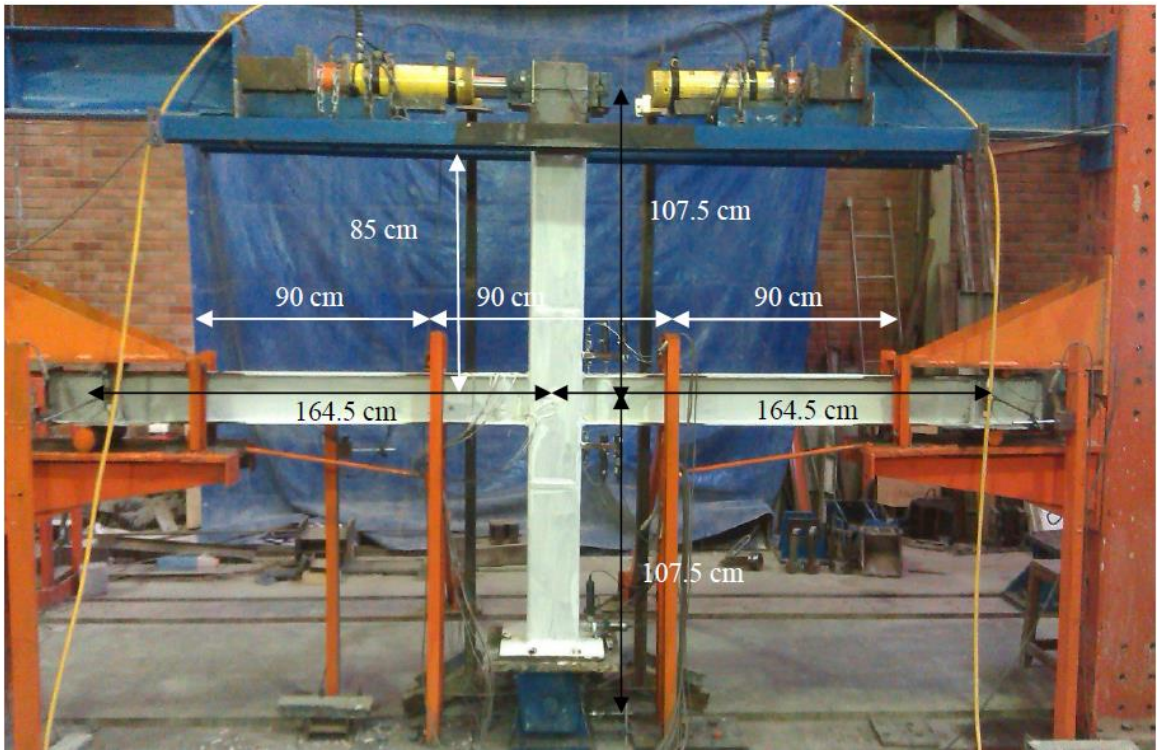

Fig. 3 Test setup configuration and overall dimensions of the specimens

specimens is shown in Fig. 3. The test setup was designed to provide expected boundary conditions for the subassemblies. The column base was fixed to the strong floor by a moment free connection and the beam ends were restrained only along the vertical direction. The cyclic load was imposed through two hydraulic actuators each with 500 kN capacity and 250 mm stroke. The applied loads were measured by two load cells installed at the back of the actuators. The out-of-plane supports were provided by applying two external frames for each beam and another one near the loading point for the column in order to avoid out-of-plane movement of the specimens, lateral-torsional buckling of beams, column rotation, and local instabilities at the loading point.

The test specimens were instrumented with a combination of linearly variable differential transformers (LVDTs) and strain gauges to measure the global and local responses. Six LVDTs were used to monitor the plastic hinge rotation and two other diagonal ones for recording shear deformations of the panel zone. Several strain gauges were pasted on the beam flange, beam web, tubes and panel zone in order to measure the history of strains in the specimens. The instrumentation is schematically shown in Fig. 4. The horizontal displacement of the actuator was measured by an external LVDT. The data sent from the LVDTs and the strain gauges were recorded using a digital data logger.

The specimens were tested by imposing a prescribed quasi-static cyclic displacement as specified in the AISC seismic provision (2010). The total story drift angle was calculated by dividing the exerted displacement by the column height. The loading history consisted of six cycles at 0.375%, 0.5% and 0.75% of total story drift angle, sequentially. The next four cycles were at 1% story drift, followed by two cycles each of successively increasing drift percentages

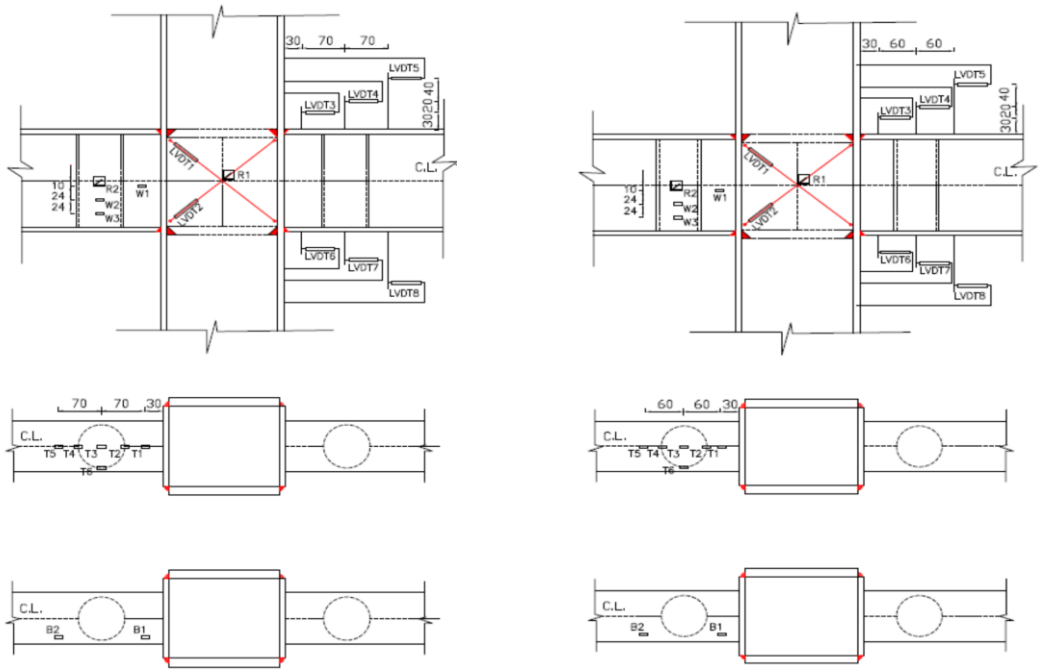

(a) SP1 (b) SP2 & SP3

Fig. 4 The location of used strain gauges and LVDTs installed on the specimens (All dimensions are in mm)

(i.e., 2, 3, 4%, etc). The cyclic tests were accomplished with a low rate in order to monitor response of the specimen in different load reversals.

4. Experimental results

4.1 Test observations

4.1.1 Test Specimen 1

The first yielding of Test Specimen 1 emerged after minor flaking of the whitewash coating of the beam top flange at the center of the reduced region during the first cycle of 1% story drift. Yielding of the beam flanges was spread over the entire reduced region after 1.5% story drift. The yielding was more extended to both sides of the reduced regions and it became apparent near the column face during story drift of 2%. During the 3% story drift, flange local buckling was observed in the reduced region as shown in Fig. 5(a). Flaking of the whitewash coating at the connections of the tubular web to the flange and the flat web near the column face was observed during the 4% story drift. As shown in Fig. 5(b), local buckling was also detected at the bottom flange of the left beam at the region close to the tubular web. In the cycles of 5% story drift, flange local buckling was much more severe in the previous regions and yielding at the tubular web extended into the full beam depth and to other regions close to the tubular web.

During the second half-cycle of the 6% story drift, cracks were initiated close to the reduced

section at the bottom flange of the left beam and at the top flange of the right beam, as depicted in Figs. 5(c) and 5(d), respectively. The crack of the bottom flange of the left beam progressed to the middle of the flange during the 4th half-cycle of the 6% story drift. The cracks progressed completely at the bottom flange of the left beam and emerged on both sides of the tube during the second half-cycle of 7% story drift as shown in Fig. 5(e). Then in the third half-cycle of 7% story drift, lateral-torsional buckling of the beam was observed. Finally, the crack of the top flange at the right beam progressed to the middle of the flange during the 4th half-cycle of 7% story drift, as shown in Fig. 5(f) and the test was terminated due to the severe fracture and considerable reduction of the bending capacity.

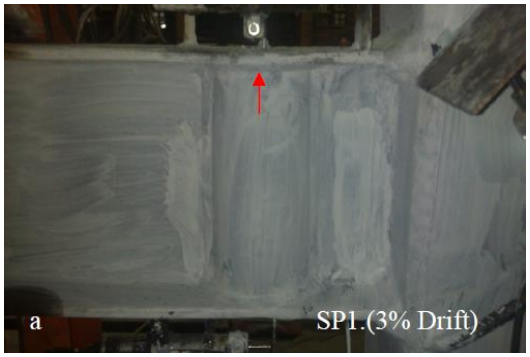

(a) Local buckling in the right beam at 3% story drift

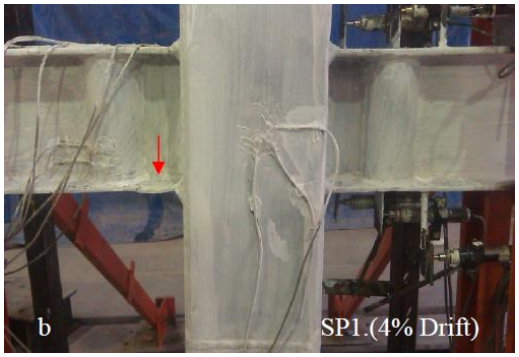

(b) Local buckling in the left beam at 4% story drift

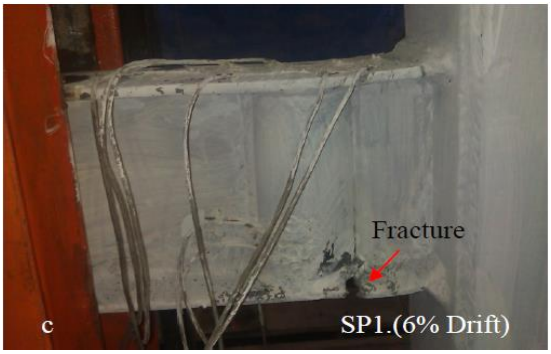

(c) Fracture in the left beam at 6% story drift

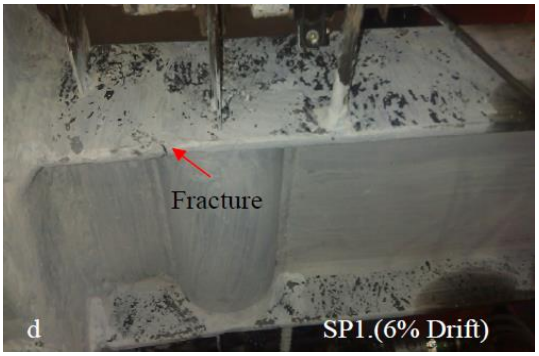

(d) Fracture in the right beam at 6% story drift

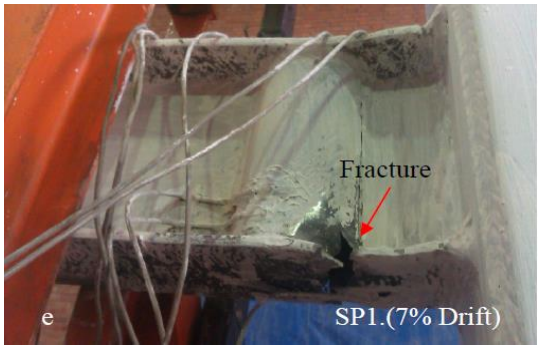

(e) Fracture in the left beam at 7% story drift

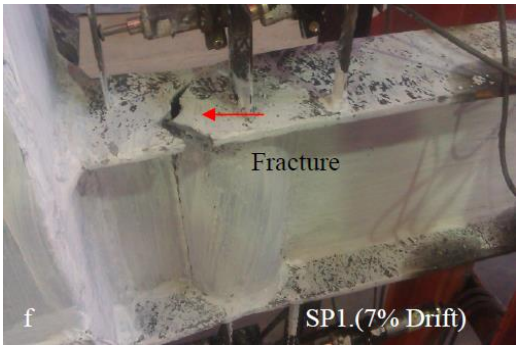

(f) Fracture in the right beam at 7% story drift

Fig. 5 Test Specimen 1 at different story drifts

4.1.2 Test Specimen 2

During the first cycle of 1% story drift, the yielding initiated at the top flange of the beams after a minor flaking at the center of the reduced region. The yielding spread over the entire reduced region at the 1.5% story drift. During the 2% story drift cycles, minor flaking was observed near the CJP welds at the bottom flange of the right beam. In the 3% story drift cycle, the yielding regions and flaking at the beam flange were more pronounced. During story drift of 4%, flange-local buckling appeared at the reduced regions of the both beams and the crack was initiated at the top flange of the right beam in front of the reduced region as shown in Fig. 6(a).

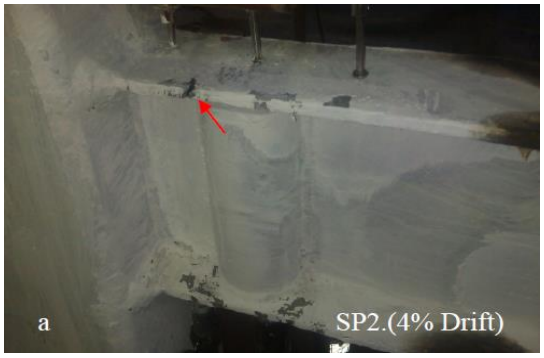

(a) Fracture in the right beam at 4% story drift

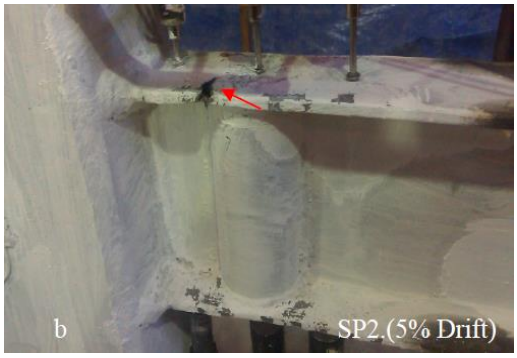

(b) Fracture in the right beam at 5% story drift

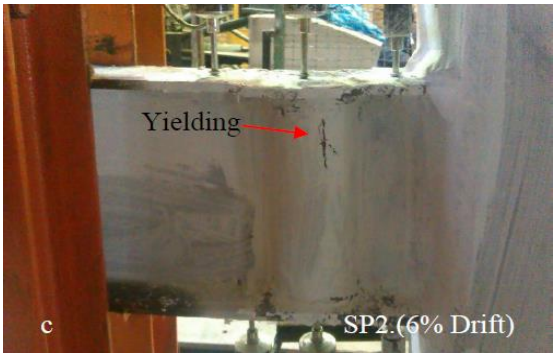

(c) yielding at the tubular web in the right beam at 6% story drift

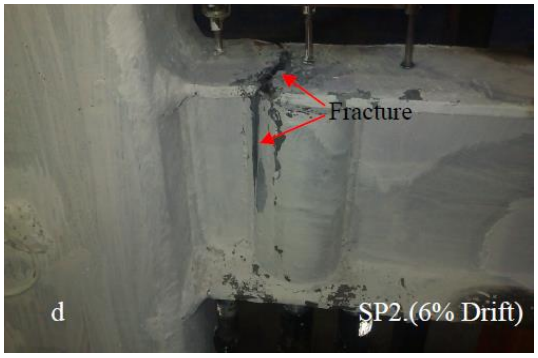

(d) Fracture in the right beam at 6% story drift

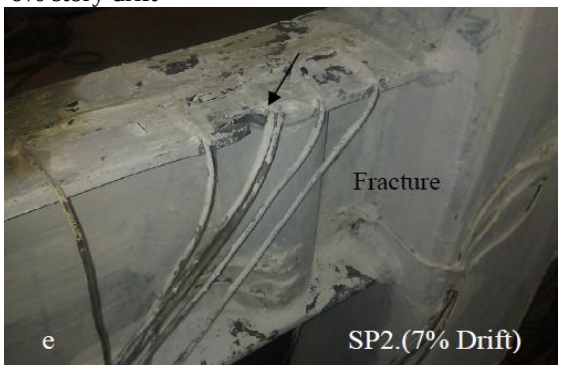

(e) Fracture in the left beam at 7% story drift

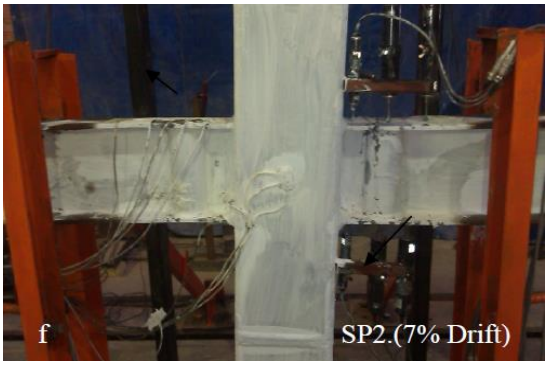

(f) specimen at the end

Fig. 6 Test Specimen 1 at different story drift

At the first cycle of 5% story drift the amplitudes of the flange buckling became more extensive at the reduced region and cracking grew along the top flange (as shown in Fig. 6(b)). Also flaking of the white wash coating at the tubular web connection to the flange and at the corner of its connection to the flat web occurred in this story drift. The crack of the top flange of the right beam progressed to the middle of the flange and fracture was initiated in the tubular web at the corner of its connection to the flat web during the second half-cycle of 6% story drift. Moreover, during this load reversal yielding was extended along depth of the tubular web, as shown in Fig. 6(c). The cracks progressed completely at the top flange of the right beam and fracture in the tube grew during the 4th half-cycle of 6% story drift as shown in Fig. 6(d). In the first half-cycle of 7% story drift, the crack was initiated at the top flange of the left beam close to the reduced region as shown in Fig. 6(e). Finally, as illustrated in Fig. 6(f), the test was terminated due to the above mentioned fractures and considerable reduction of the flexural capacity.

4.1.3 Test Specimen 3

In the SP3 specimen, the first yielding emerged on the beam flanges at the center of the reduced region during the 1% story drift. It was spread over the entire reduced region and extended toward the column face and beam end during the subsequent story drifts. In the 3% story drift, minor flaking was observed near the CJP welds at the top flange of the left beam, at the tubular web-flange connection, and also at the corner of the tubular web-flat web connection. In story drift of 4%, flange local buckling was detected at the reduced region of both top and bottom flanges of the right beam as shown in Fig. 7(a). As depicted in Figs. 7(b) to 7(f), flange local buckling would be more pronounced during the higher story drifts. Yielding of the tubular web was extended into the beam depth during the 6% story drift.

In the first cycle of 7% story drift, lateral-torsional buckling of the beam appeared in the top flange of left beam, immediately after the reduced region as shown in Fig. 7(c). In the first cycle of 8% story drift, the crack was initiated in the top flange of the left beam close to the reduced region as shown in Fig. 7(d). At the second half-cycle of 8% story drift, the previously developed crack was progressed to the middle of the flange and fracture was initiated along the tubular web-flat web connection. Fig. 7(e) shows that during the first half-cycle of 9% story drift, the cracks were progressed down along the full length of the tubular web-flat web connection. At the following second half-cycle of 9% story drift, the cracks and rupture were initiated in the bottom flange of the right beam, exactly in the reduced region as shown in Fig. 7(f). The test was terminated due to the observed fractures and the monitored reductions in the actuator force.

4.2 Investigation of the general behavior

The column tip load versus total story drift and the moment at the column face versus total plastic rotation of all specimens are shown in Fig. 8. The total story drift was calculated by dividing the column tip displacement by the distance from the column base to the centerline of the actuator. All specimens showed quite stable inelastic behaviors and favorable energy dissipation capacities throughout testing.

The results of the proposed connection satisfy AISC seismic (2010) acceptance criteria to confirm that the flexural capacity of the specimens at the column face should not be less than 80% of the beam plastic moment at 0.04 Rad and also met FEMA 350 criteria requiring to achieve a total rotation of 4% story drift before the maximum of 20% strength degradation or crack

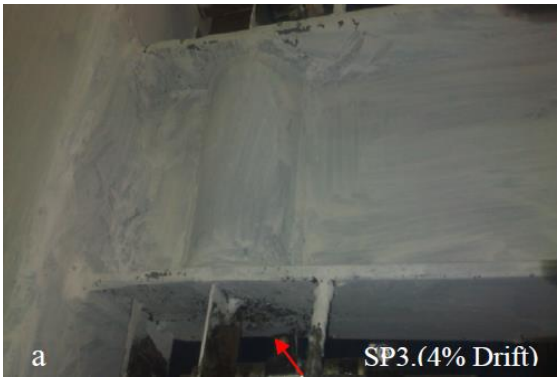

(a) Local buckling in the right beam at 4% story drift

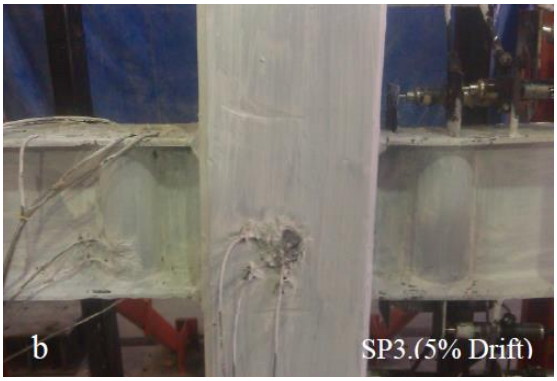

(b) Local buckling at 5% story drift

(c) Lateral-torsional buckling in the left beam at 7% story drift

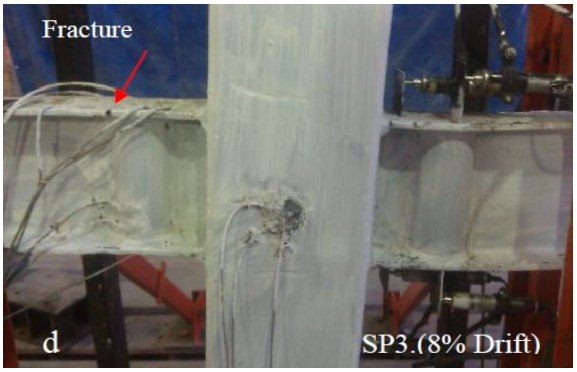

(d) Fracture in the left beam at 8% story drift

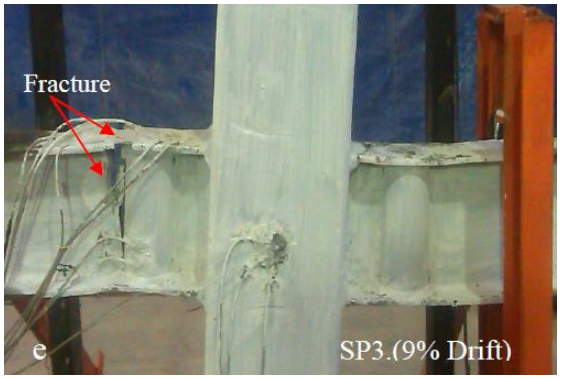

(e) Fracture in the left beam at 9% story drift

(f) Fracture in the right beam at 9% story drift

Fig. 7 Test Specimen 3 at different story drifts

occurrence in the connection and a 6% story drift before losing the total resistance. As shown in Fig. 8, 20% strength degradation was occurred at story drifts of 7%, 6%, and 9% for SP1, SP2, and SP3, respectively. In addition, the first crack was observed at story drifts of 6%, 4%, and 8%, respectively, for the SP1, SP2, and SP3. According to the obtained results, among the considered specimens, SP3 has shown the best performance in terms of displacement capacity.

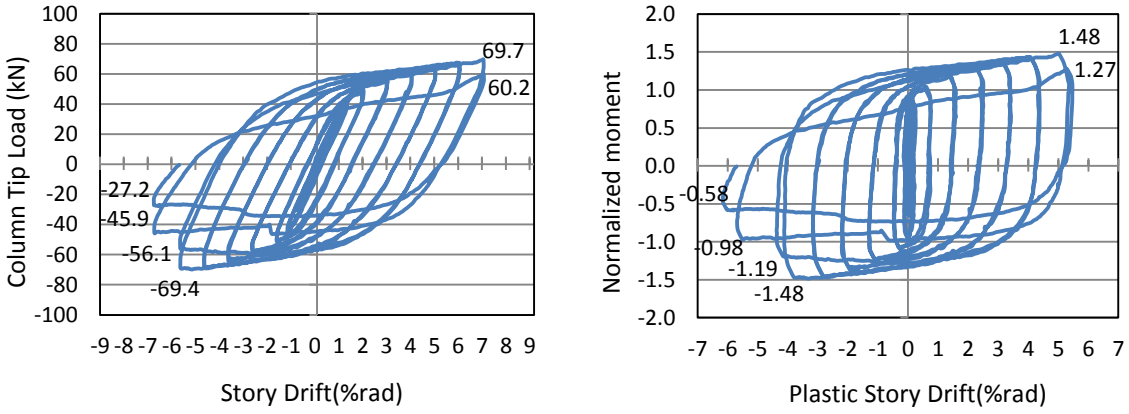

(a) TW-RBS Test Specimen 1

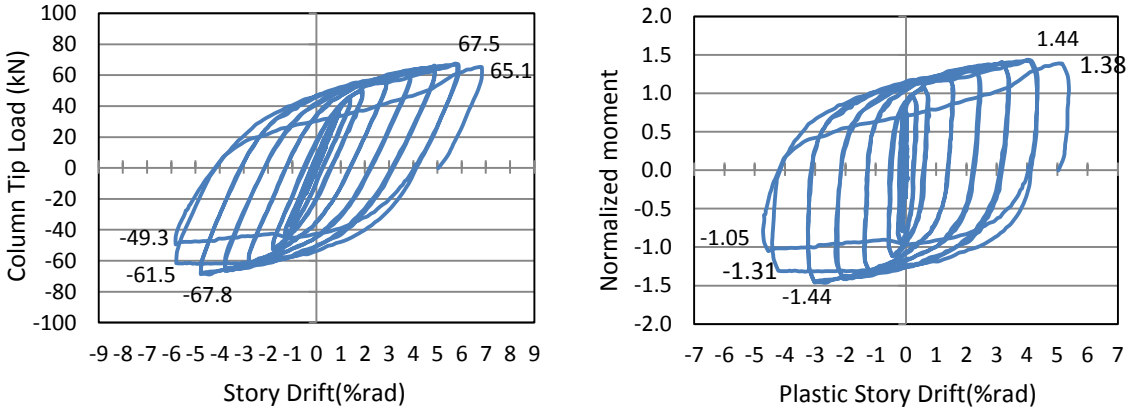

(b) TW-RBS Test Specimen 2

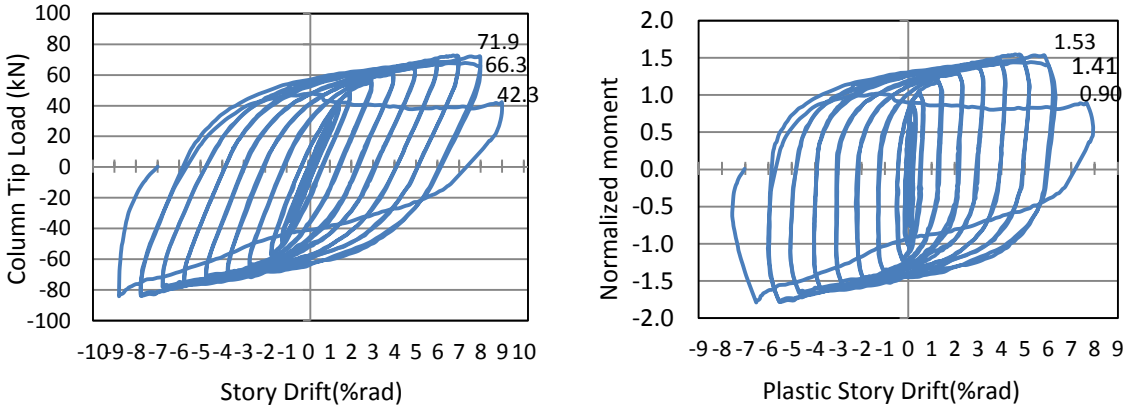

(c) TW-RBS Test Specimen 3

Fig. 8 Load versus story drift angle and normalized moment at the column face versus plastic rotation

The reason of the variations in the obtained results is mainly due to the material defects including initial defects and defects created during the specimen construction. Note that in shallow beams, flanges have commonly small dimensions such that a minor defect in the flange would lead

(a) SP1 before the loading

(b) SP1 after the rupture

(c) SP2 before the loading

(d) SP2 after the rupture

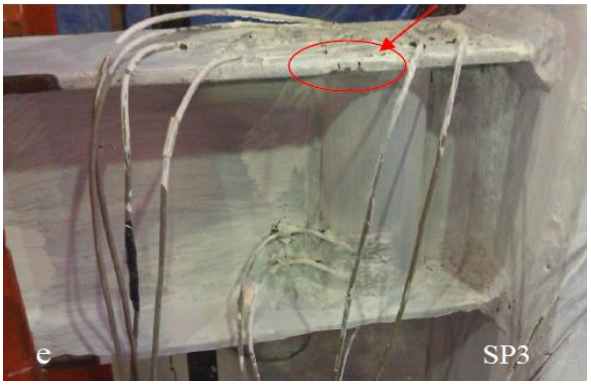

(e) SP3 before the loading

(f) SP3 after the rupture

Fig. 9 Test specimens before the loading and after the rupture

to a noticeable change in the flexural capacity of the beam. The location of the crack in beam flange and the number of cycles experienced by the specimens directly depend on such defect of materials and its amount. In Fig. 9, some pictures of specimens before the loading and after the rupture are presented. The pictures confirm the locations of failure at the parts of the specimens with initial defect of materials.

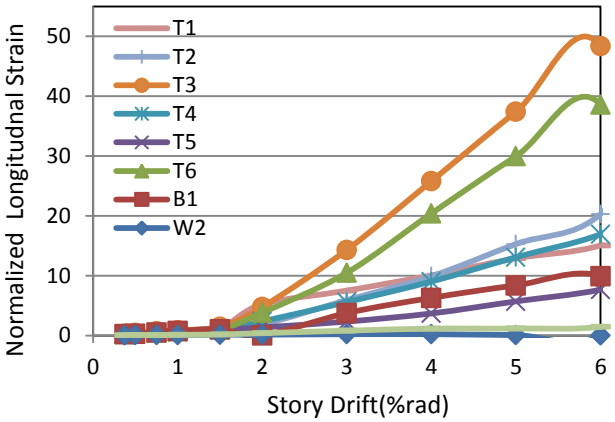

(a) TW-RBS Test Specimen 1

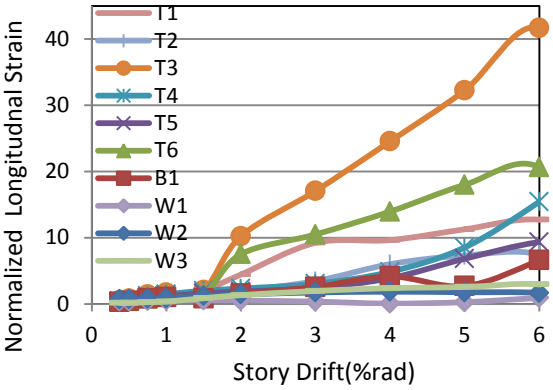

(b) TW-RBS Test Specimen 2

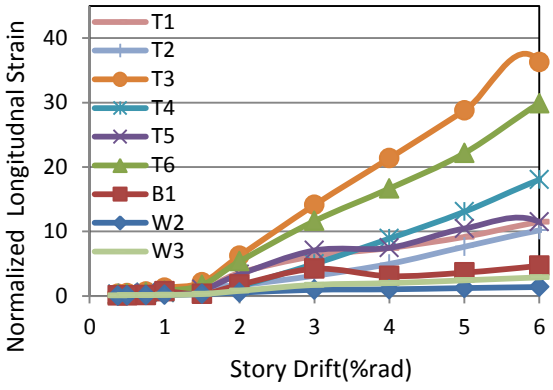

(c) TW-RBS Test Specimen 3

Fig. 10 Normalized strain profile at different strain gauges

In Fig 10, normalized strains ($\varepsilon/\varepsilon_y$) at different story drifts are presented for all TW-RBS specimens. In this figure, four strain categories can be recognized. First it presents beam flange strains at the center of reduced section (T3, T6) that has high strains and indicates concentration of plastic strains in this zone. The next category is strain of beam flange around reduced section and near the connection to column (T1, T2, T4) having a high strain level but experiencing lower strain in comparison with that of the reduced zone. The third category contains strain of beam flange in far zones from the reduced section (T5, B1) with less strain level compared to two other categories. The last category contains points on the tubular web (W1, W2, W3) showing the lowest strain level as expected having efficient match with design theories based on accordion tubular web.

In Fig. 11, normalized strains ($\varepsilon/\varepsilon_y$) at the width of the beam flange near the column face (3 cm from column face) and at the center of the reduced region (10 cm for SP1 and 9 cm for SP2 and SP3, from column face) during 4% story drift are presented. The development of the plastic hinge in the predefined region is confirmed by higher values of normalized strain at the center of reduced region in all specimens. The demand of plastic strains decreased near the column face, and therefore the possibility of fracture reduced at the beam-to-column CJP welds due to the

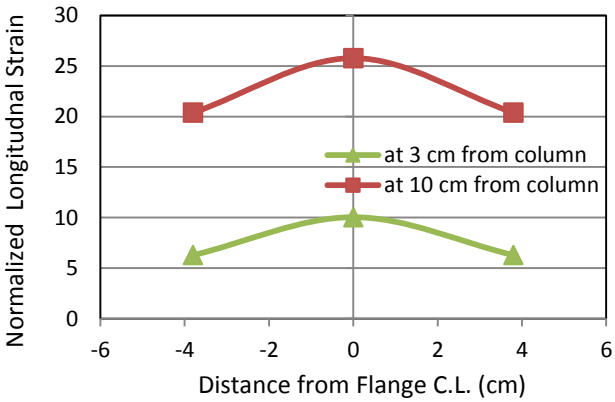

(a) TW-RBS Test Specimen 1

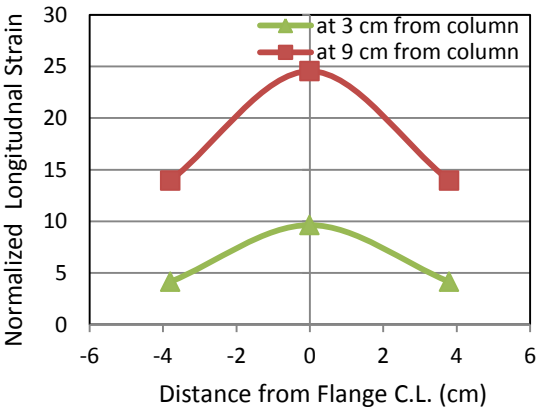

(b) TW-RBS Test Specimen 2

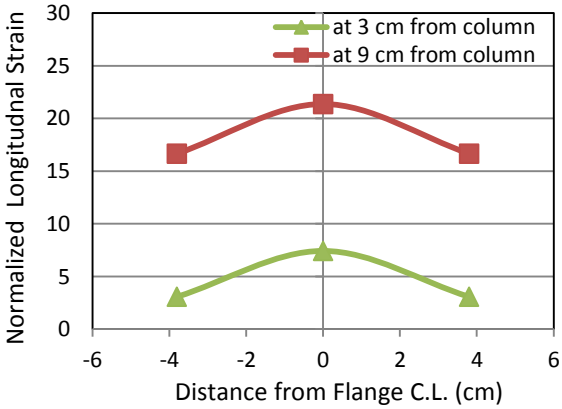

(c) TW-RBS Test Specimen 3

Fig. 11 Normalized strain profile at the width of beam flange at different distances from the column face at 4% story drift

concentration of plastic strains within the reduced region. It should be noted that during the tests no flaking of the whitewash coating was observed in the panel zone of all TW-RBS specimens even at the final stages of cyclic loading. Accordingly, the balanced behavior of the panel zone was obtained adequate and reliable.

5. Verification test and result comparison

In this section behavior of the TW-RBS connection is compared with that of the AW-RBS connection previously proposed by Mirghaderi *et al*. (2010). As mentioned earlier, AW-RBS is a kind of reduced section connection in which the accordion web configuration was provided by double angles. Different material and dimensional characteristics of the AW-RBS specimens are exactly the same as those considered for the TW-RBS connections in this study. The only difference is in the web of the reduced section region such that in AW-RBS specimens, double angles of 50×50×4 are used as the accordion web at 10 cm from column face. Therefore, it was

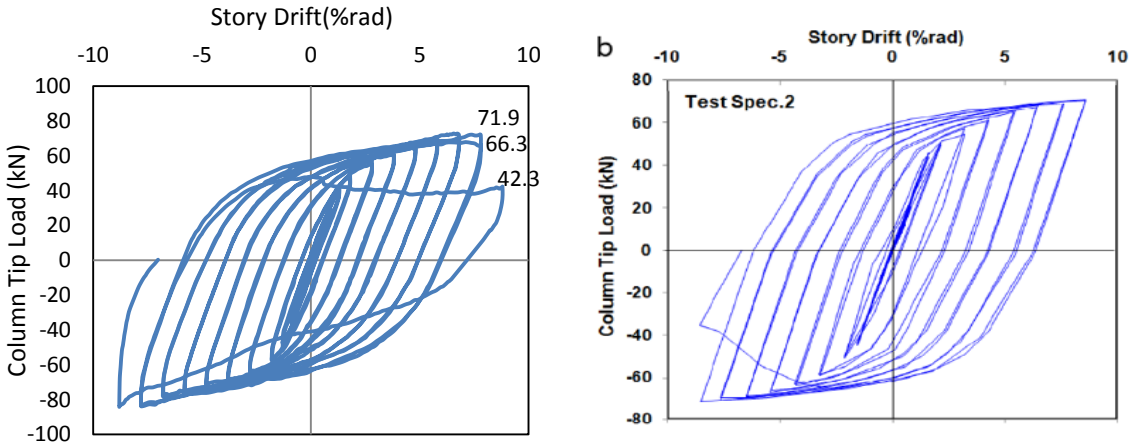

(a) TW-RBS Test Specimen (b) AW-RBS Test Specimen

Fig. 12 Comparing the experimental cyclic response of the TW-RBS specimen connection to that of the AW-RBS specimen connection

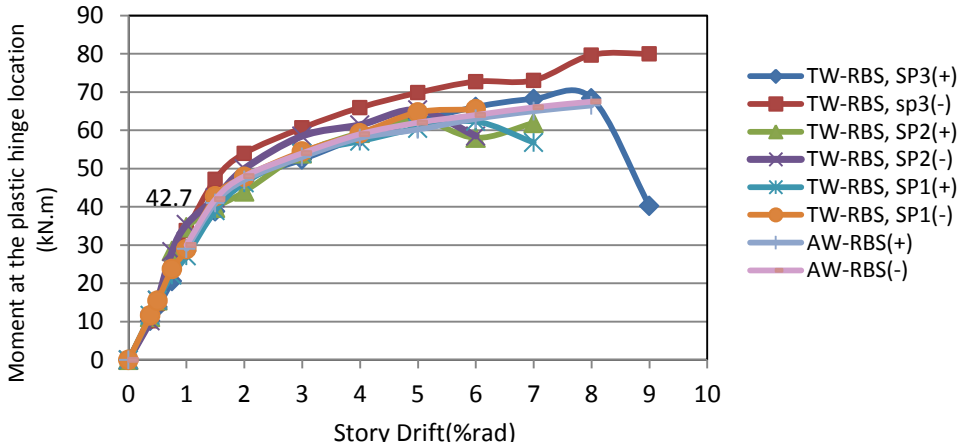

Fig. 13 Envelope curve of the beam moment at the plastic hinge location (reduced region)

considered as a suitable choice for comparison with the proposed connections.

Fig. 12 compare hysteretic behavior of the TW-RBS and the AW-RBS (Mirghaderi *et al*. 2010) connections. Both connections can sustain significant ductility demands up to 8% story drift without reducing the flexural strength at the column face. According to this figure the TW-RBS connection satisfies AISC seismic provisions (2010) and FEMA (2000) acceptance criteria up to 9% story drift however the AW-RBS connection experiences more than 20% strength degradation at 8% story drift.

In Fig. 13, envelope behavior of the TW-RBS and AW-RBS connections are compared. According to this figure, TW-RBS and AW-RBS connections have the same behavior. According to Fig. 13 moment of 42.7kN.m was developed in the plastic hinge region of the TW-RBS specimens. The plastic moment of full section of the beam is about 54 kN.m, and the ratio of the amount of plastic moment in plastic hinge to the plastic moment of the beam is 0.79. Also the ratio

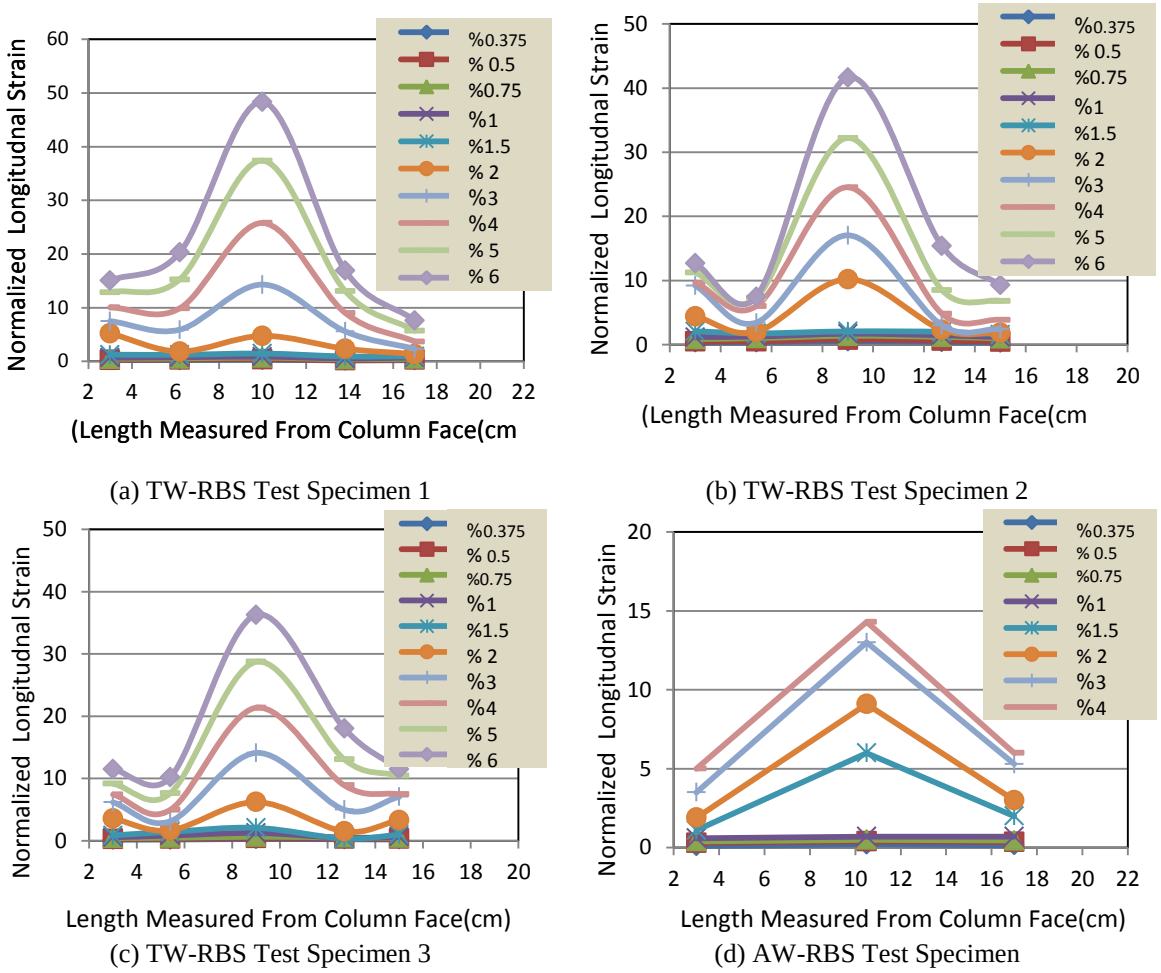

(a) TW-RBS Test Specimen 1

(b) TW-RBS Test Specimen 2

(c) TW-RBS Test Specimen 3

(d) AW-RBS Test Specimen

Fig. 14 Normalized longitudinal strain profile along the beam top flange

of $Z_{AW\text{-}RBS}$ to beam plastic section modulus (Z_b) is 0.79 (as reported in Tables 2 and 3). This verifies the proposed design method presented in Table 3.

The longitudinal strain envelopes of the beam top flanges in the cases of TW-RBS and AW-RBS connections are compared in Fig. 14. The formation of the plastic hinge in the predefined region is confirmed by higher values of normalized strain, developed in the flanges within the reduced section in all specimens. Evaluating the values presented in the curve shows that strain of flange in the reduced section zone of the proposed connection is over three times the strains near the column face. For AW-RBS, normalized strain at 0.02, 0.03 and 0.04 radian story drifts at the reduced region were obtained to be 9, 13 and 14, respectively; whereas these values are, on average, 9, 16 and 23 for the TW-RBS connection in the reduced region at the same story drift representing an increase of plastic strain concentration in the reduced region of the TW-RBS compared to AW-RBS connection.

Normalized strains at accordion webs of the TW-RBS and AW-RBS connections are presented in Fig. 15. The behaviors of all specimens are similar. As clearly shown, strain profile in tubular

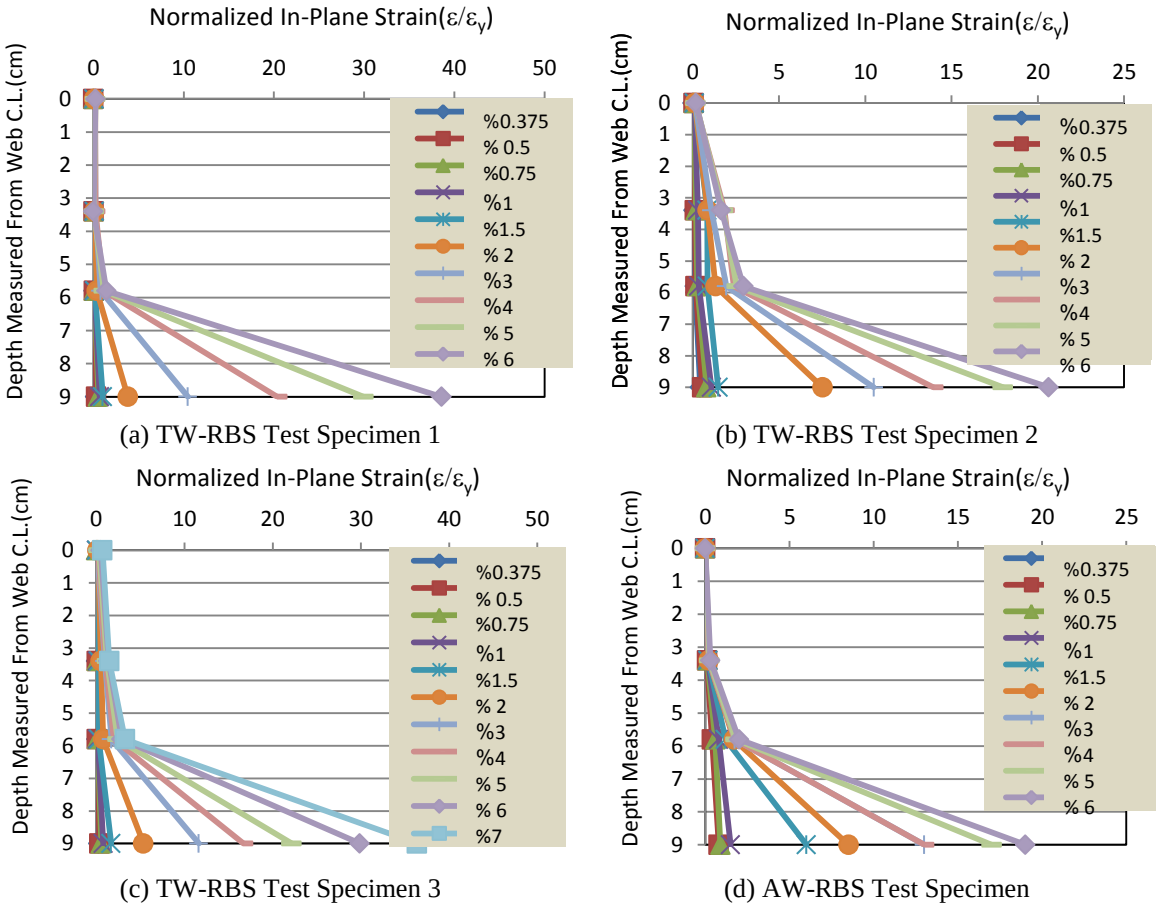

(a) TW-RBS Test Specimen 1

(b) TW-RBS Test Specimen 2

(c) TW-RBS Test Specimen 3

(d) AW-RBS Test Specimen

Fig. 15 Envelope of normalized strain at different distances from the neutral axis at the tubular web

web has a significant decrease in comparison with linear profile of strain distribution in flat web and the tubular web behavior has caused great reduction in the axial strain of the web at the plastic hinge location. According to the curves, axial strain in the tubular web increased close to the beam flange; while this value is quite small at the mid-height of the beam.

This low longitudinal strain in web leads to elimination of the web contribution to the flexural capacity of the beam. Among the different specimens, SP1 with tubular web having smaller thickness and lower yield strength has softer accordion behavior and impose more tension on the beam flange at the reduced region. For example, SP1 at 6% story drift shows normalized strain close to 40 while the corresponding values of SP2 and SP3 were in the range of 20 to 30. AW-RBS has flange normalized strain of less than 20 at 6% story drift showing less ductility on its accordion behavior.

6. Numerical study

In this section hysteretic behavior of the proposed TW-RBS connection is numerically

simulated to explore further details about its response during load reversals.

6.1 Finite element modeling and analysis

Connections analysis is carried out using a three-dimensional finite element model in ABAQUS. The geometry and mechanical properties of finite element models are exactly the same as those used for the tested specimens. All components are modeled with shell elements. Four-node quadrilateral element for tube and tetrahedral element for other components with six degrees of freedom was used for meshing the components. Mesh size of all components is similar (maximum dimension of 1.5 cm) except for the beam flange in which smaller mesh size was considered (maximum dimension of 1.25 cm). All regarded elements are square-shaped and degrees of freedom in the connection zones were bound together with Tie constraints. The yield strength (F_y) and the ultimate strength (F_u) of the materials were considered as per the tensile coupon test results, as summarized in Table 2. The Young modulus of elasticity and Poisson ratio were assumed as 203 GPa and 0.3, respectively for all materials of the analysis. A cyclic displacement with increasing amplitude, similar to the experimental loading protocol, was incrementally imposed to the column tip of the numerical model.

6.2 Numerical result verification

The numerical cyclic behaviors of the specimens are in good agreement with those obtained from the experiments, as shown in Fig. 16. The deformed shape and the plastic strain distribution for TW-RBS SP1 at 4% story drift are shown in Fig. 17. The results show that plastic hinge is formed at the flange in the centers of accordion areas. The plastic strain in the surrounding corrugated area such as CJP welds has far less intensity.

Fig. 18 shows numerical results of the strain envelopes of the top flange along the longitudinal direction. The numerical results are correlated suitably by experimental results of TW-RBS specimens, as shown in Fig. 14. The formation of the plastic hinge in the predefined region is

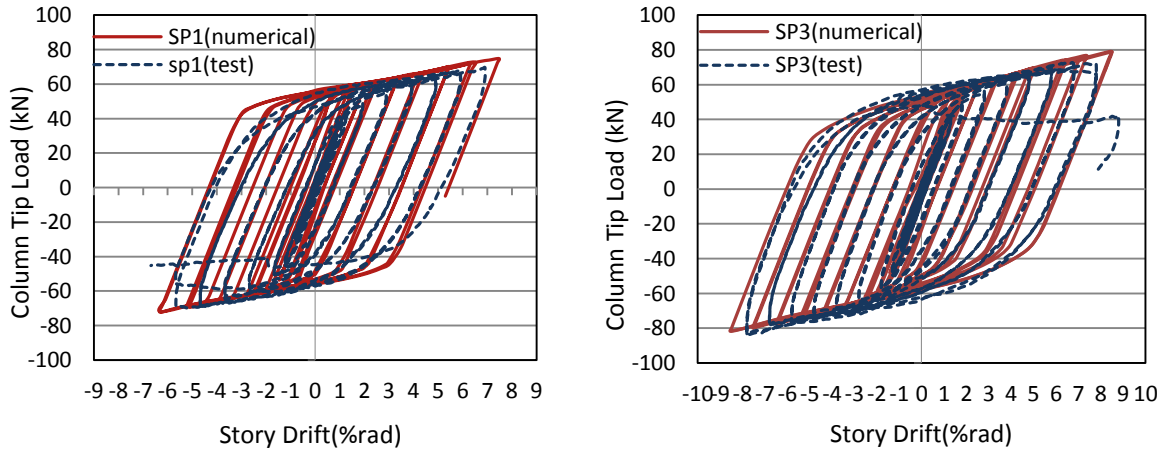

(a) TW-RBS Test Specimen 1 (b) TW-RBS Test Specimen 3

Fig. 16 Result verification of numerical analysis compared to experimental results of TW-RBS

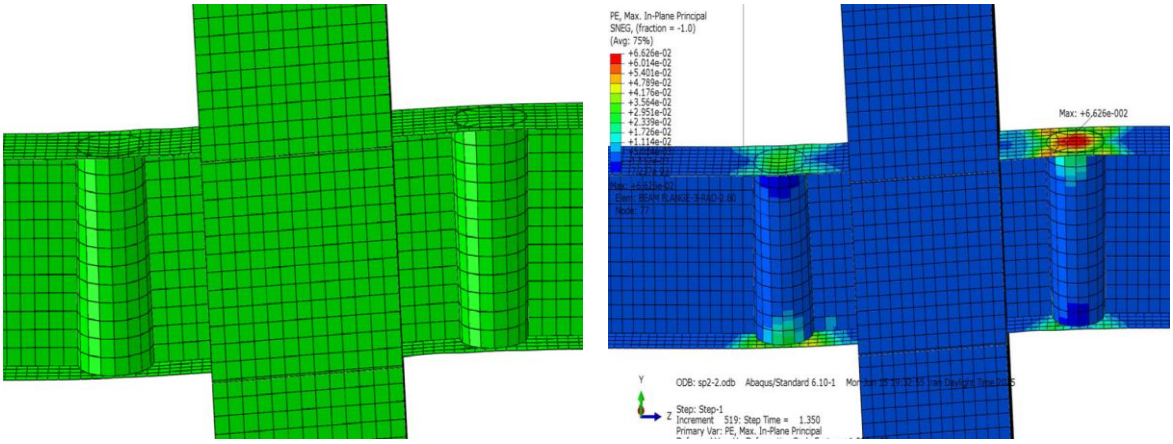

(a) Deformed shape (b) Von Mises plastic strain distribution.

Fig. 17 Numerical results of TW-RBS test specimen 1 at 4% story drift

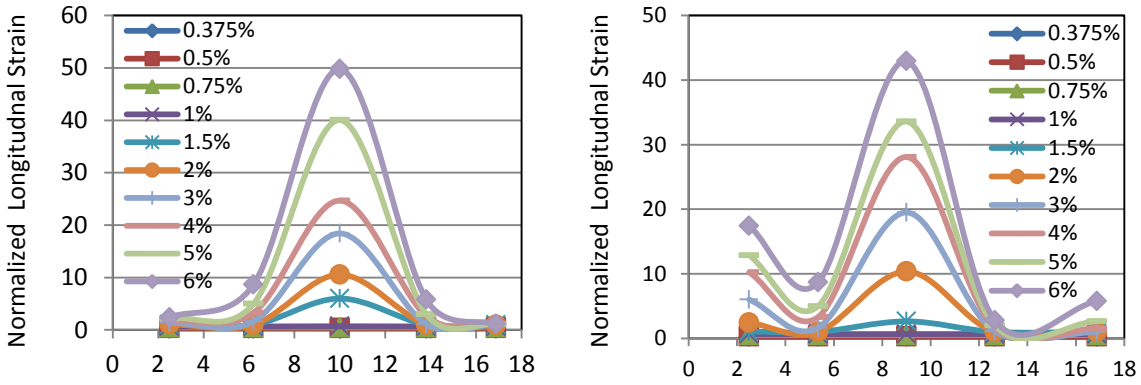

(a) TW-RBS Test Specimen 1 (b) TW-RBS Test Specimen 2 & 3

Fig. 18 Numerical results of the normalized longitudinal strain profile along the beam top flange

confirmed by higher values of normalized strain, developed in the flanges within the reduced section.

6.3 Comparison with conventional RBS

A numerical model of conventional RBS connection with circular cutting of flange and a rigid beam to column connection is used here for validation of TW-RBS connection. The Dimensions of the adopted substructure and the size of used beam and column are exactly the same as those used in the TW-RBS connection tests. In order to design the RBS beam, the parameter α (demand ratio of flexural capacities) is selected to be 90% similar to that used for the TW-RBS specimens. In the RBS connection, a circular cut of connection begins from 6.75 cm at the column face and length of the cut is 15 cm. The highest reduction in flange width in reduced section is 35%. The material type is selected similar to that used for the TW-RBS specimens.

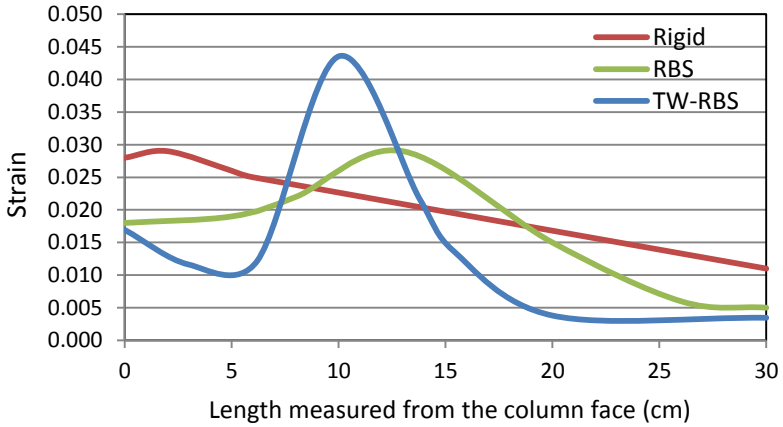

Fig. 19 Strain at 0.06 radian story drift at midfield of beam tensile flange

According to the results, in the conventional RBS local buckling of the web and the flanges in the reduced zone appeared at the story drift of 3%. The web lateral-torsional buckling also appeared in cycles of 4% story drift. In Fig. 19, the strain distributions are compared in the midfield of the tensile beam flange in all three connections at 0.06 radian story drift. According to the objectives of reduced section connections, the strain demand on the beam-to-column connections is reduced significantly, whereas in the rigid connections, the maximum strain occurs at the column face increasing the risk of brittle failure. Conventional RBS connection and AW-RBS almost have reduced the same amount of strain at the beam-to-column connections while the TW-RBS has significantly reduced strain of the column face in beam-to-column connection area. This confirms that the TW-RBS connection would lead to more strain concentration within the reduced section which is a beneficial feature. Also, conventional RBS connection has a more uniform strain distribution while the connection with accordion web has effectively concentrated the plastic strains in the reduced section zone and it has resulted in less strain demands on the beam-to-column connection.

7. Conclusions

In this study, a new type of RBS connection, called TW-RBS, was proposed in typical shallow beams and its hysteretic behavior was evaluated experimentally and numerically. In the TW-RBS connection, the flat beam web would be replaced by a tube at the desired location of the plastic hinge. The results indicate that because of the accordion-like behavior of the web, the contribution of the beam web to the plastic hinge capacity becomes smaller and almost negligible. Due to this localized flexural strength reduction, TW-RBS can effectively concentrate the plastic strains within the reduced region and result in substantial reduction in the developed strain demands near the critical CJP welds. The main findings of the present study can be summarized as following:

- TW-RBS at shallow beams can provide significant ductility up to 8% story drift without reducing the flexural strength at the column face and can easily satisfy AISC seismic provisions (2010) and FEMA (2000) acceptance criteria.
- Flange local buckling was detected inside the reduced region and lateral-torsional buckling

appeared only in high story drift (7%) in the TW-RBS connection at shallow beams showing an improvement in the out-of-plane stiffness and stability condition of plastic hinge.

• Compared with the previously developed AW-RBS, TW-RBS has superior performance in terms of low-cycle fatigue. This stems with the fact that the change of strain direction in arc shape of the tabular web creates smaller angles compared to the sharp corners of the AW-RBS's accordion web. On this basis and due to experimental observations, beginning of failure at the AW-RBS connection occurs at the accordion web in sharp corners of angles while in the case of TW-RBS connection the failures were all triggered at the flange of the reduced region rather than the accordion web.

• The proposed connection has softer accordion behavior compared to that of the AW-RBS. This leads to more strain concentration at the flange of the reduced section. Using tubular web with smaller thickness or lower yield strength in the TW-RBS connection makes the accordion behavior even more ductile.

Acknowledgments

Authors would like to thank the University of Tehran for supporting this research project (8108020/1/08) and the BHRC (Building and Housing Research Center) of Iran for conducting the experimental work. Their assistance is highly appreciated.

References

American Institute of Steel Construction (2010), Seismic Provisions for Structural Steel Buildings, AISC, Chicago.

Engelhardt, M., Winneberger, T., Zekany, A. and Potyraj, T. (1998), "Experimental investigation of Dogbone moment connections", *Eng. J. AISC*, Fourth Quarter, 128-139.

Federal Emergency Management Agency (2000), FEMA-350, Seismic design criteria for new moment resisting steel frame construction, Washington DC.

Federal Emergency Management Agency (2000), FEMA-355D, State of the art report on connection performance, Washington DC.

Han, S.W. and Moon, H.H. (2009), "Design equations for moment strength of RBS-B connection", *J. Constr. Steel Res.*, **65**, 1087-1095.

Mirghaderi, S.R., Torabian, S. and Imanpour, A. (2010), "Seismic performance of the Accordion-Web RBS connection", *J. Constr. Steel Res.*, **66**, 277-288.

Morrison, M., Schweizer, D. and Hassan, T. (2015), "An innovative seismic performance enhancement technique for steel building moment resisting connections", *J. Constr. Steel Res.*, **109**, 34-46.

Naeim, F. (2001), *The seismic design handbook*, 2nd Edition, Kluwer Academic Publishers.

Pachoumis, D.T., Galoussis, E.G., Kalfas, C.N. and Efthimiou, I.Z. (2010), "Cyclic performance of steel moment-resisting connections with reduced beam sections-experimental analysis and finite element model simulation", *Eng. Struct.*, **32**(9), 2683-2692.

Ricles, J.M., Mao, C., Lu, L.W. and Fisher, J.W. (2003), "Ductile details for welded unreinforced moment connections subject to inelastic cyclic loading", *Eng. Struct*., **25**(5), 667-680.

Saleh, A., Mirghaderi, S.R. and Zahrai, S.M. (2016a), "Cyclic testing of tubular web RBS connections in deep beams", *J. Constr. Steel Res.*, **117**, 214-226.

Saleh, A., Zahrai, S.M. and Mirghaderi, S.R. (2016b), "Cyclic testing of tubular web RBS connections with two accordion cells in deep beams", *Eng. Struct.* (in Press)

Tsavdaridis, K.D. and D'Mello, C. (2012), "Optimisation of novel elliptically-based web opening shapes of perforated steel beams", *J. Constr. Steel Res.*, **76**, 39-53.
Wilkinson, S., Hurdman, G. and Crouther, A. (2006), "A moment resisting connection for earthquake resisting structure", *J. Constr. Steel Res.*, **62**, 295-302.
Yang, Q. and Yang, N. (2009), "Seismic behaviors of steel moment resisting frames with opening in beam web", *J. Constr. Steel Res.*, **65**(6), 1323-1336.

PL